Bioconjugate Chemistry

Article

pubs.acs.org/bc

Delivery of a Protease-Activated Cytolytic Peptide Prodrug by Perfluorocarbon Nanoparticles

Andrew P. Jallouk,[†] Rohun U. Palekar,[†] Jon N. Marsh,[†] Hua Pan,[†] Christine T. N. Pham,[‡] Paul H. Schlesinger,[§] and Samuel A. Wickline*[,†,§]

[†]Consortium for Translational Research in Advanced Imaging and Nanomedicine, Division of Cardiology, Department of Medicine, Washington University in St. Louis School of Medicine, St. Louis, Missouri 63108, United States

[‡]Division of Rheumatology, Department of Medicine and [§]Department of Cell Biology and Physiology, Washington University in St. Louis School of Medicine, St. Louis, Missouri 63110, United States

Supporting Information

ABSTRACT: Melittin is a cytolytic peptide derived from bee venom that inserts into lipid membranes and oligomerizes to form membrane pores. Although this peptide is an attractive candidate for treatment of cancers and infectious processes, its nonspecific cytotoxicity and hemolytic activity have limited its therapeutic applications. Several groups have reported the development of cytolytic peptide prodrugs that only exhibit cytotoxicity following activation by site-specific proteases. However, systemic administration of these constructs has proven difficult because of their poor pharmacokinetic properties. Here, we present a platform for the design of protease-activated melittin derivatives that may be used in conjunction with a perfluorocarbon nanoparticle delivery system. Although native melittin was substantially hemolytic (HD_{50}: 1.9 μM) and cytotoxic (IC_{50}: 2.4 μM), the prodrug exhibited 2 orders of magnitude less hemolytic activity (HD_{50}: > 100 μM) and cytotoxicity (IC_{50}: > 100 μM). Incubation with matrix metalloproteinase-9 (MMP-9) led to cleavage of the prodrug at the expected site and restoration of hemolytic activity (HD_{50}: 3.4 μM) and cytotoxicity (IC_{50}: 8.1 μM). Incubation of the prodrug with perfluorocarbon nanoparticles led to stable loading of 10 250 peptides per nanoparticle. Nanoparticle-bound prodrug was also cleaved and activated by MMP-9, albeit at a fourfold slower rate. Intravenous administration of prodrug-loaded nanoparticles in a mouse model of melanoma significantly decreased tumor growth rate ($p = 0.01$). Because MMPs and other proteases play a key role in cancer invasion and metastasis, this platform holds promise for the development of personalized cancer therapies directed toward a patient's individual protease expression profile.

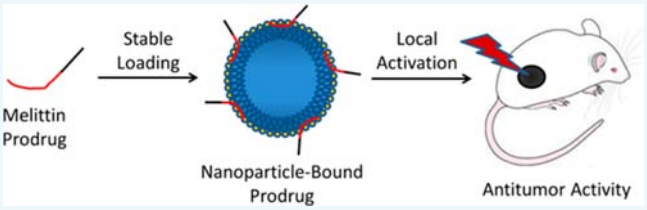

INTRODUCTION

Melittin is a cytolytic peptide derived from bee venom that inserts into lipid membranes and oligomerizes to form membrane pores.[1] The broad applicability of this mechanism of action makes melittin a versatile tool for the destruction of harmful biological entities such as cancer cells,[2,3] bacteria,[4,5] and viruses.[6,7] Furthermore, unlike conventional chemotherapeutic agents, melittin limits the development of resistance by targeting the overall structure of the membrane rather than a particular cellular component.[8] Yet, the therapeutic applications of melittin have been limited by its nonspecific cytotoxicity and hemolytic activity. Several delivery strategies have been proposed to minimize these off-target effects, including incorporation of melittin onto a nanoparticle carrier.[9−11] In particular, perfluorocarbon nanoparticles have been shown to reduce melittin toxicity to sperm and vaginal epithelium in vitro[12] and allow intravenous administration of melittin at doses exceeding its LD_{50} with no harmful effects.[3] To further enhance the safety of this treatment, however, there is interest in developing melittin derivatives that exhibit cytolytic activity only at a specified site following activation.

Several groups have previously reported the development of protease-activated cytolytic peptide derivatives.[13−16] Although these constructs vary in their design and intended applications, all demonstrate substantial activity when locally applied to the appropriate environment. However, systemic administration of these compounds has proven difficult because of their rapid renal clearance and lack of accumulation in tissues of interest. To address these issues, we have designed a platform for generating protease-activated melittin derivatives that take advantage of a perfluorocarbon nanoparticle delivery system for localization of therapeutic activity.

The melittin prodrug design is based on the structure of honeybee promelittin,[17] a natural precursor of melittin that is not cytolytic but still exhibits strong noncovalent interactions with perfluorocarbon nanoparticles. These nanoparticles, in turn, function as versatile carriers that may be targeted to sites of interest and that have previously been shown to enhance melittin circulation time and accumulation within tumors.[3] For

Received: April 30, 2015
Revised: June 15, 2015
Published: June 17, 2015

DOI: 10.1021/acs.bioconjchem.5b00246
Bioconjugate Chem. 2015, 26, 1640−1650

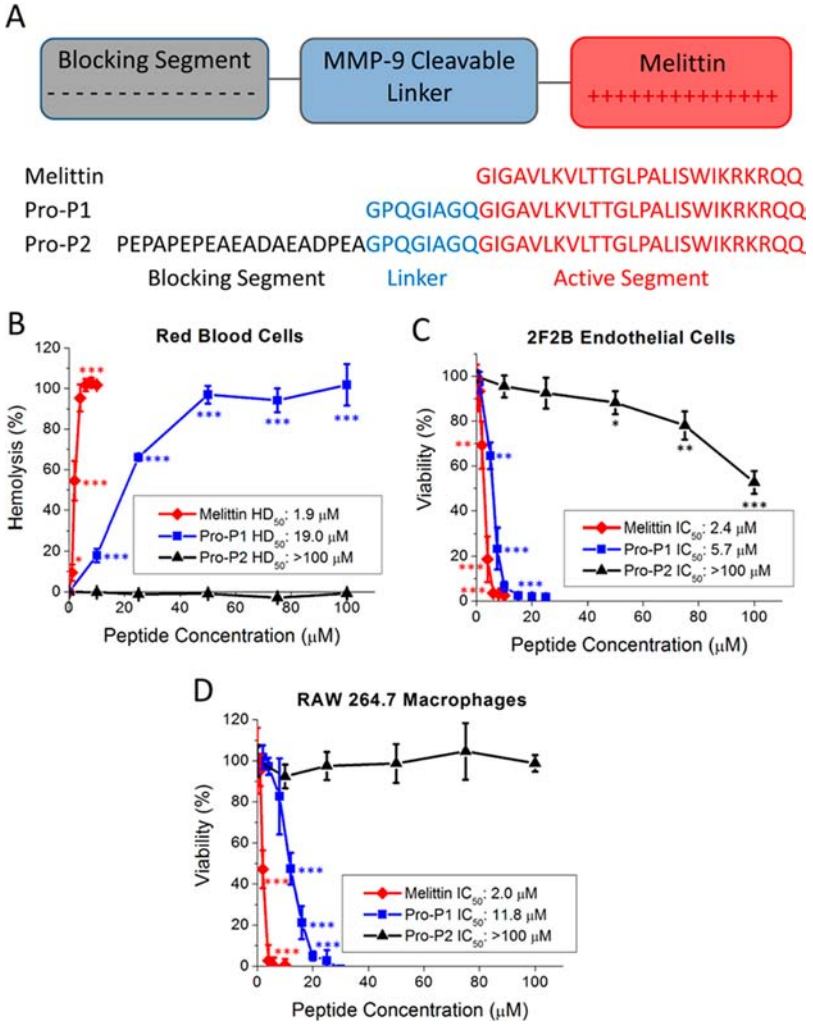

Figure 1. Structure and cytolytic activity of melittin derivatives. (A) Design and sequence of melittin prodrug. Hemolytic activity and cytotoxicity of melittin prodrug to (B) red blood cells, (C) 2F2B endothelial cells, and (D) RAW 264.7 macrophages following incubation for 3 h. Error bars represent standard deviation of $n = 6$ replicates. Labels indicate level of statistical significance compared to untreated control: *, $p < 0.05$; **, $p < 0.01$; and ***, $p < 0.001$.

proof-of-concept, we synthesized a melittin derivative that could be activated by matrix metalloproteinase-9 (MMP-9), a protease that is overexpressed in many tumors and that plays a critical role in cancer invasion and metastasis.[18,19] We then characterized the loading and activation of this prodrug on perfluorocarbon nanoparticles and demonstrated for the first time in vivo the efficacy of a cytolytic peptide prodrug under conditions of systemic administration with a nanoparticle drug delivery system. Given the recent interest in personalized cancer therapy,[20,21] this platform could be used to generate a panel of melittin prodrugs that would be selectively administered to patients on the basis of their individual patterns of tumor protease expression.

RESULTS AND DISCUSSION

Prodrug Cytolytic Activity. As shown in Figure 1A, the prodrug consists of a glutamate-/proline-rich blocking segment joined to the N terminus of melittin via an MMP-9 cleavable linker sequence. This blocking segment is modeled after honeybee promelittin to incorporate its actions as an inhibitor of melittin cytolytic activity. This inhibition has been extensively characterized by truncation analysis.[15] As with other blocking segments used in similar applications,[16,22] its inhibitory effect on melittin correlates highly with its length and magnitude of negative charge. To demonstrate this inhibition, we assessed the toxicity of N-terminally functionalized melittin derivatives to several cell types commonly encountered in the cardiovascular system (Figures 1B–D). Native melittin exhibited substantial hemolytic activity (HD_{50}: 1.9 ± 0.1 μM) and cytotoxicity to 2F2B endothelial cells (IC_{50}: 2.4 ± 0.2 μM) and RAW 264.7 macrophages (IC_{50}: 2.0 ± 0.1 μM). Addition of the short linker sequence alone (Pro-P1) slightly decreased hemolytic activity (HD_{50}: 19.0 ± 0.6 μM) and cytotoxicity (2F2B IC_{50}: 5.7 ± 0.1 μM; RAW IC_{50}: 11.8 ± 0.4 μM), whereas addition of the complete blocking segment (Pro-P2) reduced hemolytic activity ($HD_{50} \gg 100$ μM) and cytotoxicity (2F2B $IC_{50} > 100$ μM; RAW $IC_{50} \gg 100$ μM) by at least 2 orders of magnitude. No significant hemolytic activity was observed at prodrug concentrations up to 100 μM. These results clearly demonstrate the effectiveness of the blocking segment for inhibiting melittin cytolytic activity.

Importantly, the modular nature of this prodrug design permits substitution of individual components as needed, thereby facilitating prodrug development for a wide variety of applications. For instance, the linker sequence used in this

DOI: 10.1021/acs.bioconjchem.5b00246
Bioconjugate Chem. 2015, 26, 1640–1650

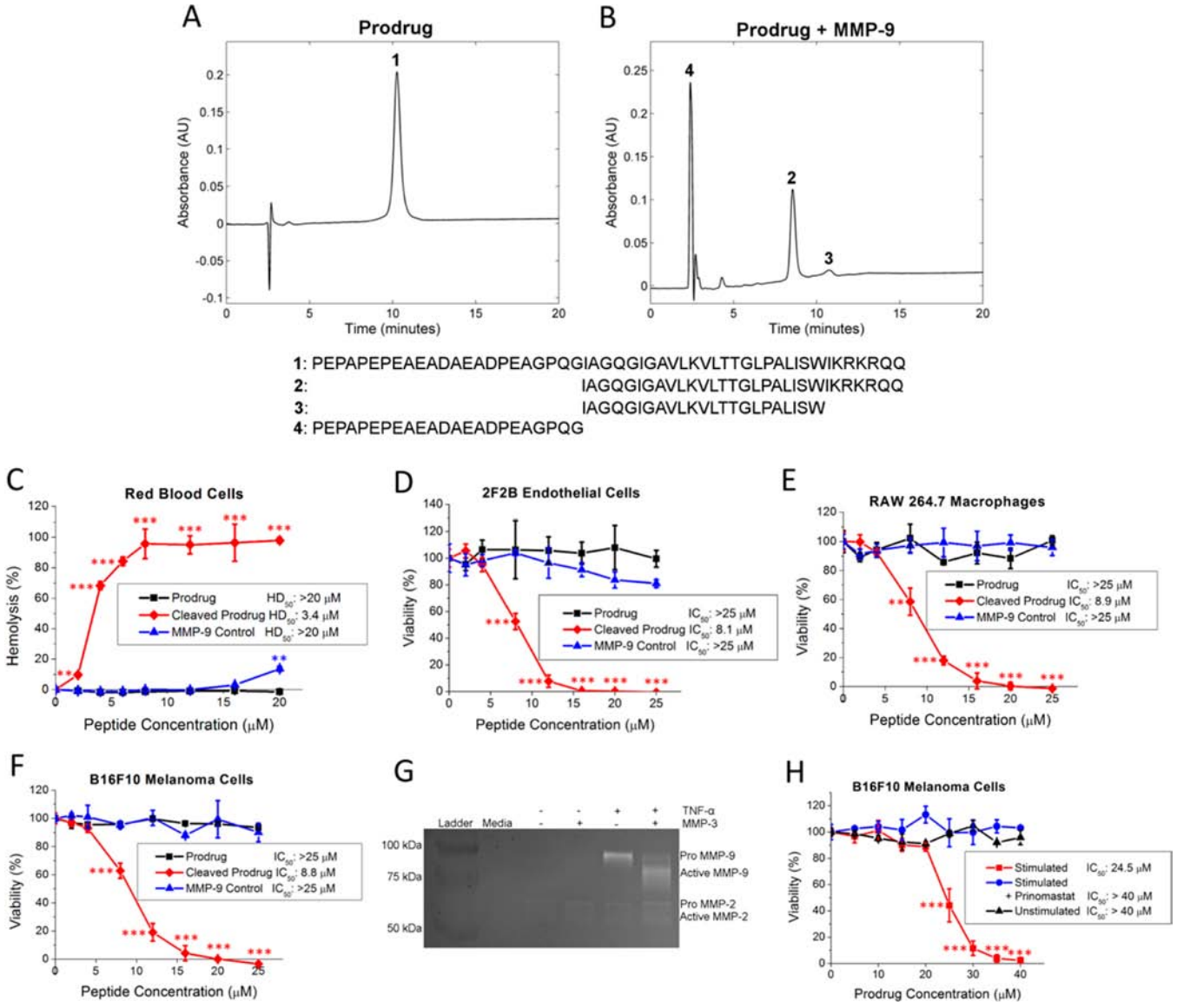

Figure 2. Prodrug cleavage and activation by MMP-9. (A) Chromatogram of uncleaved prodrug. (B) Chromatogram of prodrug following incubation for 3 h with 20 nM active MMP-9. Hemolytic activity and cytotoxicity of cleaved and uncleaved prodrug to (C) red blood cells, (D) 2F2B endothelial cells, (E) RAW 264.7 macrophages, and (F) B16F10 melanoma cells following incubation for 3 h. (G) Gelatin zymogram demonstrating MMP-9 production following stimulation of B16F10 melanoma cells with TNF-α and MMP-3. (H) Cytotoxicity of prodrug to stimulated B16F10 melanoma cells following incubation for 3 h. Error bars represent standard deviation of $n = 3$ replicates. Labels indicate level of statistical significance compared to untreated control: *, $p < 0.05$; **, $p < 0.01$; and ***, $p < 0.001$.

study is derived from collagen and is rapidly cleaved by gelatinases such as MMP-9.[23] However, the cleavage kinetics of a multitude of other short peptides have also been characterized,[24,25] and these sequences may be included as linkers on the basis of their susceptibility to cleavage by a particular combination of proteases. This flexibility makes the prodrug platform ideal for the development of personalized cancer therapies that are based on the results of individual protease expression profiling.[26,27] Similarly, although the use of melittin as an anticancer therapeutic has been repeatedly demonstrated,[3,10] other peptide toxins could be substituted as needed for particular applications. Because many peptide toxins require cationic residues to exert their membrane-disrupting effects,[28] it is possible that anionic blocking segments such as that derived from promelittin could serve as broadly applicable inhibitors of cytolytic activity. Nevertheless, the precise structural requirements for successful inhibition have yet to be thoroughly characterized and may vary by toxin or require additional design considerations.

Prodrug Cleavage and Activation. Prodrug cleavage following exposure to recombinant MMP-9 was characterized by reversed-phase high-performance liquid chromatography (HPLC). As shown in Figure 2A, uncleaved prodrug eluted in a single peak with a retention time of approximately 10.3 min (peak 1). Incubation with 20 nM recombinant MMP-9 for 3 h resulted in the appearance of a distinct second peak with retention time 8.6 min (Figure 2B, peak 2). Mass spectrometry confirmed the identity of this peak as the expected product following cleavage of the linker sequence. Another minor peak with retention time 10.8 min (peak 3) was noted in HPLC data and found by mass spectrometry to represent a distinct peptide cleaved at both the expected linker site and at the C-terminal

DOI: 10.1021/acs.bioconjchem.5b00246
Bioconjugate Chem. 2015, 26, 1640−1650

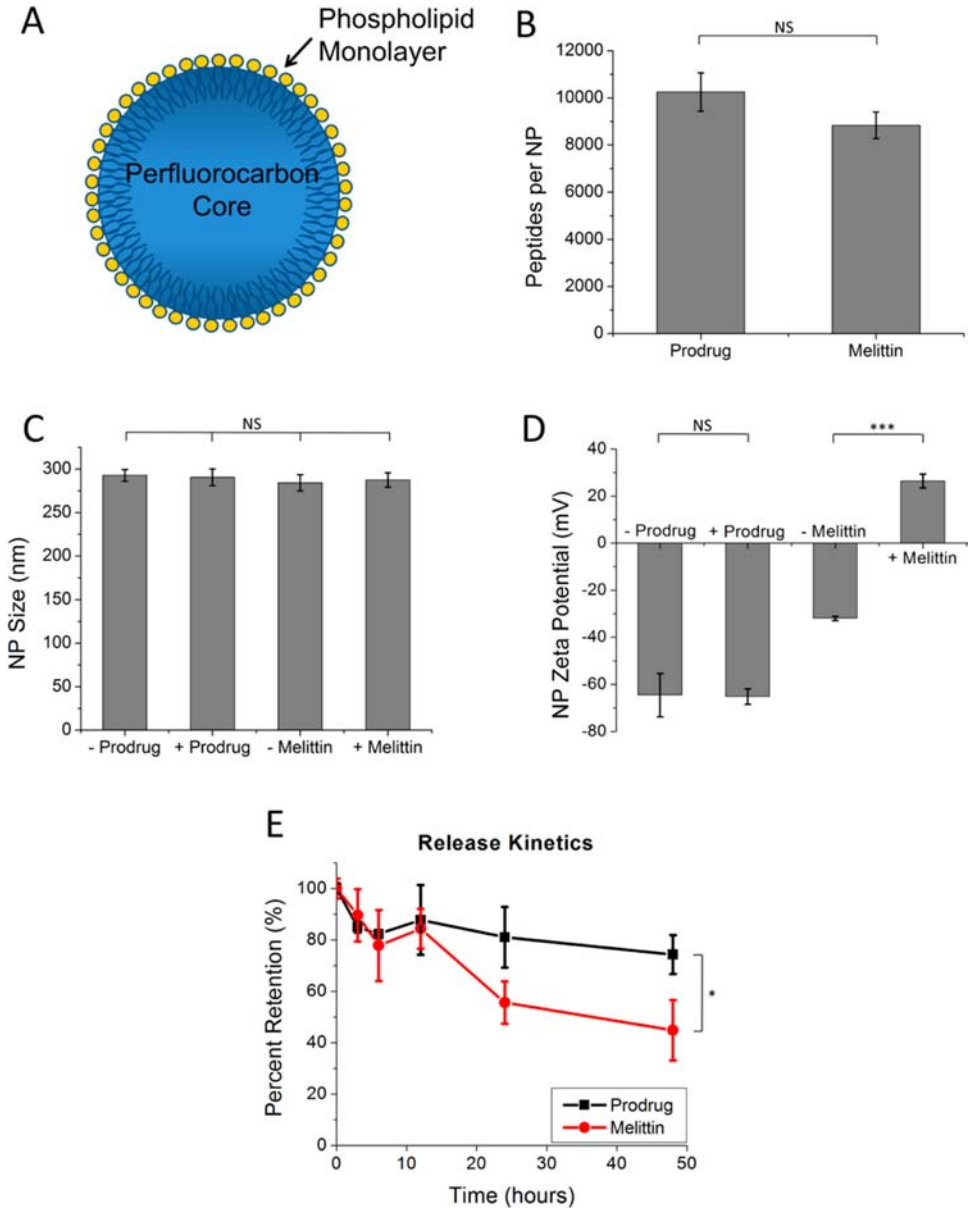

Figure 3. Prodrug and melittin loading of perfluorocarbon nanoparticles. (A) Schematic diagram of a perfluorocarbon nanoparticle. (B) Stable loading of perfluorocarbon nanoparticles by prodrug and melittin following three washes with buffer. (C) Nanoparticle size following prodrug and melittin loading. (D) Nanoparticle zeta potential following prodrug and melittin loading. (E) Release kinetics of nanoparticles loaded with prodrug or melittin during dialysis against an infinite sink. Error bars represent standard deviation of $n = 3$ replicates. Labels indicate level of statistical significance between groups: NS, $p > 0.05$; *, $p < 0.05$; and ***, $p < 0.001$.

end of the tryptophan in the melittin sequence. The hydrophilic blocking segment eluted at approximately 2.4 min (peak 4). Addition of the MMP-9 inhibitor prinomastat to the solution prevented cleavage of the prodrug under similar conditions (Figure S1). The prominence of the peaks representing the expected cleavage products and the lack of other substantial peaks in the chromatogram indicate that MMP-9 cleaves the prodrug predominantly at the expected site in the linker sequence. The presence of the doubly cleaved product in peak 3, however, suggests that additional cleavage events are possible. Given the crucial role of the cationic C-terminal residues in the interaction of melittin with cell membranes,[29] this doubly cleaved species is likely to be substantially less cytotoxic than native melittin. Thus, cleavage at alternate sites could serve as a mechanism for prodrug degradation and elimination. Further tuning of this process could be accomplished via incorporation of modified linkages or unnatural amino acids in the prodrug sequence.

To determine whether cleavage by MMP-9 restored functional activity of the melittin prodrug, we assessed the cytotoxicity and hemolytic activity of fully cleaved prodrug on a variety of cell lines (Figures 2C–F). Cleaved prodrug demonstrated substantial hemolytic activity (HD_{50}: 3.4 ± 0.1 μM) and cytotoxicity to 2F2B endothelial cells (IC_{50}: 8.1 ± 0.2 μM), RAW 264.7 macrophages (IC_{50}: 8.9 ± 0.8 μM), and B16F10 melanoma cells (IC_{50}: 8.8 ± 0.8 μM). In contrast, neither uncleaved prodrug nor recombinant MMP-9 alone exhibited similar cytotoxicity or hemolytic activity profiles (HD_{50}: > 25 μM; IC_{50}: > 25 μM for all cell lines). Although these results indicate a clear restoration of cytolytic activity

DOI: 10.1021/acs.bioconjchem.5b00246
Bioconjugate Chem. 2015, 26, 1640–1650

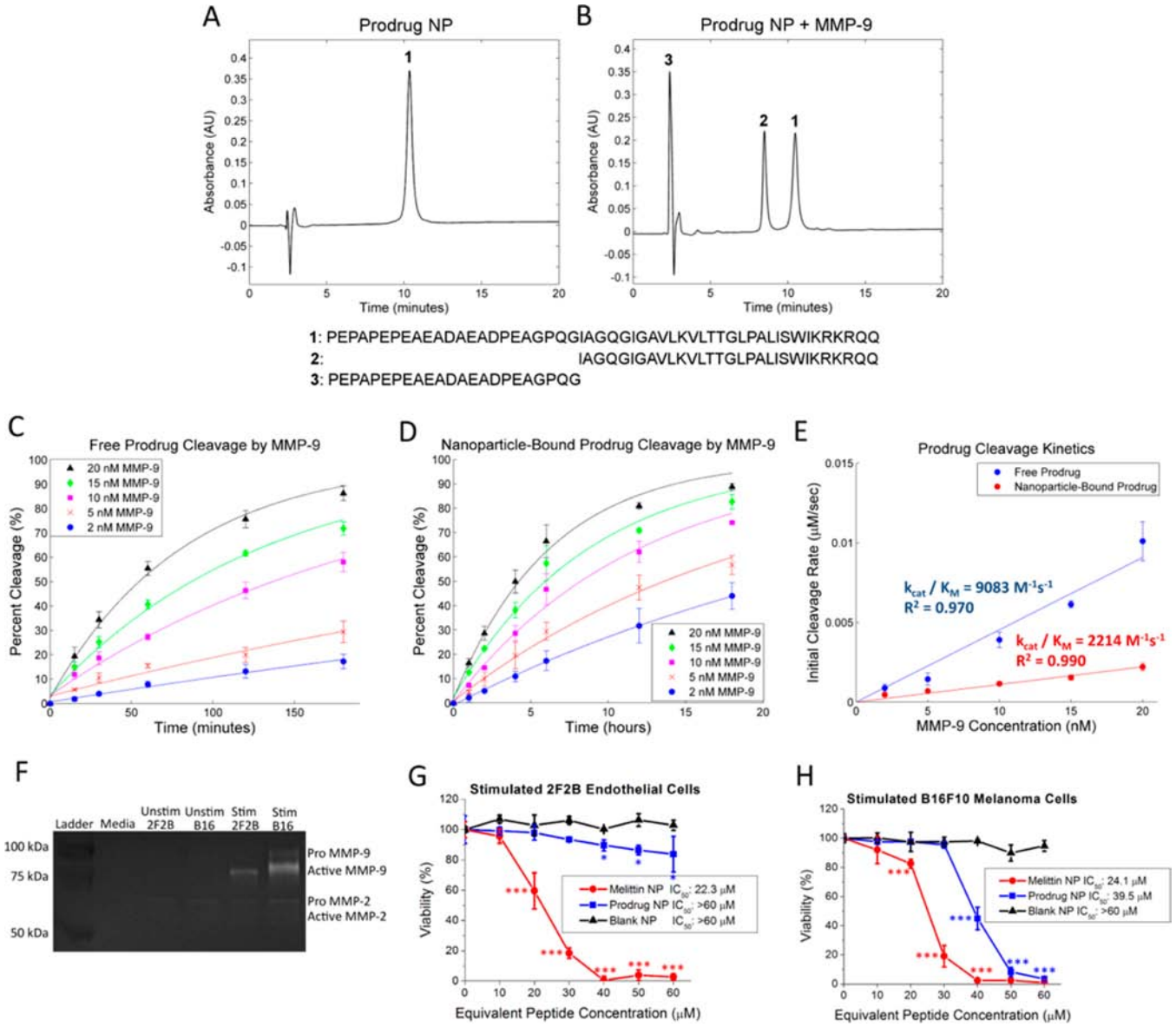

Figure 4. Cleavage and activation of nanoparticle-bound prodrug by MMP-9. (A) Chromatogram of prodrug-loaded nanoparticles. (B) Chromatogram of prodrug-loaded nanoparticles following incubation for 3 h with 20 nM MMP-9. (C) Cleavage kinetics of 50 μM free prodrug by MMP-9. (D) Cleavage kinetics of 50 μM nanoparticle-bound prodrug by MMP-9. (E) Determination of k_{cat}/K_m constant for free and nanoparticle-bound prodrug cleavage by MMP-9. (F) Gelatin zymogram demonstrating MMP-9 production following TNF-α and MMP-3 stimulation of 2F2B endothelial cells and B16F10 melanoma cells. (G) Cytotoxicity of nanoparticles loaded with melittin or prodrug to stimulated 2F2B endothelial cells following incubation for 24 h. (H) Cytotoxicity of nanoparticles loaded with melittin or prodrug to stimulated B16F10 melanoma cells following incubation for 24 h. Error bars represent standard deviation of $n = 3$ replicates. Labels indicate level of statistical significance compared to untreated control: *, $p < 0.05$; **, $p < 0.01$; and ***, $p < 0.001$.

following MMP-9 cleavage, the activated prodrug does not appear to be quite as toxic as native melittin (Figure 1). This difference arises from the four N-terminal residues remaining on the melittin sequence following MMP-9 cleavage of the prodrug. Upon binding to membranes, this region of melittin transitions from a random coil to an α-helical conformation that is necessary for subsequent oligomerization and pore formation.[28] Thus, it is not surprising that the presence of additional N-terminal residues would impact the ability of melittin to disrupt cellular membranes. Although the precise structural changes that lead to this disruption have yet to be determined, extension of α-helix length or steric interference with oligomerization could serve as potential mechanisms.

Production of active MMPs by tumors is a complex process that often involves cytokine-induced secretion of latent proenzymes which are activated extracellularly by proteases generated from tumor-associated stroma or immune cells.[19] In particular, tumor necrosis factor-α (TNF-α) has been shown to stimulate production of proMMP-9 by B16F10 melanoma cells,[30] and MMP-3 has been identified as an important activator of proMMP-9.[31,32] Thus, in order to assess prodrug activation by cell-produced MMP-9, we stimulated B16F10 melanoma cells with a combination of TNF-α and MMP-3. Gelatin zymography demonstrated appearance of a ~90 kDa band representing proMMP-9 upon addition of TNF-α (Figure 2G). Further addition of MMP-3 diminished the intensity of this band and resulted in the appearance of multiple ~80 kDa

DOI: 10.1021/acs.bioconjchem.5b00246
Bioconjugate Chem. 2015, 26, 1640−1650

bands representing active MMP-9 species. As shown in Figure 2H, the melittin prodrug was toxic to B16F10 melanoma cells stimulated in this fashion (IC_{50}: 24.5 ± 0.5 μM) but not to unstimulated cells (IC_{50}: > 40 μM). Addition of the MMP-9 inhibitor prinomastat eliminated toxicity to stimulated cells (IC_{50}: > 40 μM), further emphasizing the importance of MMP-9 activity for activation of the prodrug. Together, these results demonstrate the successful development of a melittin prodrug which exhibits MMP-9 dependent cytolytic activity.

Nanoparticle Loading and Activation. As shown in Figure 3A, perfluorocarbon nanoparticles consist of a hydrophobic perfluorocarbon core surrounded by a phospholipid monolayer that may be covalently functionalized with targeting ligands or serve as a reservoir for lipophilic drugs. Native melittin has been shown to stably insert into the phospholipid monolayer without disrupting nanoparticle structure, allowing these nanoparticles to serve as efficient in vivo delivery vehicles for melittin.[3,9] Incorporation onto perfluorocarbon nanoparticles increases the plasma half-life of melittin from 24 min to over 300 min and improves the safety profile of melittin treatment by facilitating clearance of circulating peptide through the reticuloendothelial system.[3] Furthermore, magnetic resonance imaging has demonstrated persistent accumulation of perfluorocarbon nanoparticles within tumors several hours following systemic administration.[33] These pharmacokinetic improvements are especially important for the delivery of melittin prodrugs that must be retained in tissues for significant periods of time in order to be activated and exert their cytolytic effect.

Through incorporation of 10% dipalmitoylphosphatidylglycerol into the phospholipid monolayer, we developed a nanoparticle formulation which stably loaded 10 250 peptides per nanoparticle following simple incubation with the prodrug (Figure 3B). This value corresponded to a loading efficiency of 35.1%. For comparison, we applied the same analysis technique to loading of native melittin onto the previously reported nanoparticle formulation containing 2% dipalmitoylphosphatidylethanolamine.[3,9] Simple incubation of these nanoparticles with melittin led to stable loading of 8840 peptides per nanoparticle (loading efficiency = 24.5%). Importantly, these loading assessments were performed following three washes with buffer, which resulted in an undetectable level of free prodrug and native melittin remaining in solution. Neither addition of prodrug nor addition of melittin significantly altered nanoparticle size (Figure 3C; prodrug: $p = 0.77$; melittin: $p = 0.68$). In contrast, although addition of prodrug did not significantly alter nanoparticle zeta potential (Figure 3D; $p = 0.91$), addition of melittin led to a dramatic reversal of zeta potential from −32.0 mV to 26.4 mV ($p < 0.001$). This difference is likely due to the cationic nature of native melittin and the relative neutralization of charge in the prodrug caused by the anionic blocking segment. To characterize peptide release from nanoparticles, we dialyzed nanoparticles loaded with prodrug or native melittin against an infinite sink of phosphate-buffered saline (PBS; Figure 3E). There was no significant loss of either peptide within 12 h (prodrug: 87.8 ± 13.5% retention, $p = 0.20$; melittin: 84.3 ± 7.7% retention, $p = 0.06$), further supporting the use of these nanoparticles as systemic delivery agents. After 48 h, 74.3% of prodrug and 44.8% of melittin remained nanoparticle-bound. Although noncovalent interactions between promelittin and phospholipid membranes have previously been reported,[34] the mechanism of these interactions appears complex and is currently under further investigation. Nevertheless, the persistence of high levels of nanoparticle-bound prodrug following three washes and extended exposure to infinite sink conditions demonstrates for the first time that these interactions may be sufficient to allow nanoparticle-mediated delivery of peptides derived from promelittin.

To characterize the cleavage and activation of nanoparticle-bound prodrug, we incubated prodrug-loaded nanoparticles with recombinant MMP-9 following three washes with buffer to remove unbound prodrug. Nanoparticles were then treated with isopropanol to remove the perfluorocarbon and subjected to HPLC analysis in order to determine the peptide species present. As we found for the free peptide, uncleaved prodrug eluted in a single peak with a retention time of approximately 10.3 min (Figure 4A, peak 1). Incubation with 20 nM recombinant MMP-9 for 3 h resulted in the appearance of a distinct second peak with a retention time of 8.5 min, representing the expected cleavage product (Figure 4B, peak 2). Although these results demonstrate that nanoparticle loading does not alter the site of cleavage by MMP-9, the persistence of a substantial amount of uncleaved prodrug (Figure 4B, peak 1) indicates that cleavage of nanoparticle-bound peptide proceeds more slowly than cleavage of the peptide in solution as shown in Figure 2. To compare the cleavage kinetics of prodrug in solution versus nanoparticle-bound prodrug, we incubated these constructs with MMP-9 concentrations ranging from 2 to 20 nM and studied the time course of cleavage from 30 to 180 min for free prodrug (Figure 4C) and 1−18 h for nanoparticle-bound prodrug (Figure 4D). We then used the initial cleavage rate as a function of MMP-9 concentration to calculate an effective k_{cat}/K_m constant, a measure of catalytic efficiency, for free and nanoparticle-bound prodrug. As shown in Figure 4E, the effective k_{cat}/K_m for free prodrug was 9083 M^{-1} s^{-1}, compared to 2214 M^{-1} s^{-1} for nanoparticle-bound prodrug, indicating that nanoparticle-bound prodrug was cleaved at a rate approximately fourfold slower than that of free prodrug. We suggest that this slower cleavage profile is likely to be beneficial in vivo by further minimizing any nonspecific activation that might occur in the bloodstream while still permitting activation during extended residence times in tissues of interest.

In contrast to other nanoparticle platforms that deliver active toxins, one key advantage of the melittin prodrug system is the lack of toxicity toward tissues that do not express the targeted protease. To further reinforce this point, we compared the cytotoxicity of melittin-loaded nanoparticles and prodrug-loaded nanoparticles following TNF-α/MMP-3 stimulation of 2F2B endothelial cells and B16F10 melanoma cells. As shown in Figure 4F, neither 2F2B nor B16F10 cells expressed a detectable level of MMP-9 before stimulation. Upon stimulation, however, B16F10 cells produced a substantially greater amount of active MMP-9 than did 2F2B cells. This difference is reflected in their prodrug cytotoxicity profiles because prodrug-loaded nanoparticles were cytotoxic to B16F10 cells (IC_{50}: 39.5 ± 0.4 μM) at concentrations lower than those that were cytotoxic to 2F2B cells (IC_{50}: > 60 μM, Figures 4G−H). In contrast, melittin-loaded nanoparticles were cytotoxic to both cell lines at similar concentrations (2F2B cells: IC_{50}: 22.3 ± 1.6 μM; B16F10 cells: 24.1 ± 0.6 μM). Blank nanoparticles exhibited no detectable cytotoxicity to either cell line (2F2B cells: IC_{50}: > 60 μM; B16F10 cells: IC_{50}: > 60 μM). These results again demonstrate the efficacy and selectivity of

DOI: 10.1021/acs.bioconjchem.5b00246
Bioconjugate Chem. 2015, 26, 1640−1650

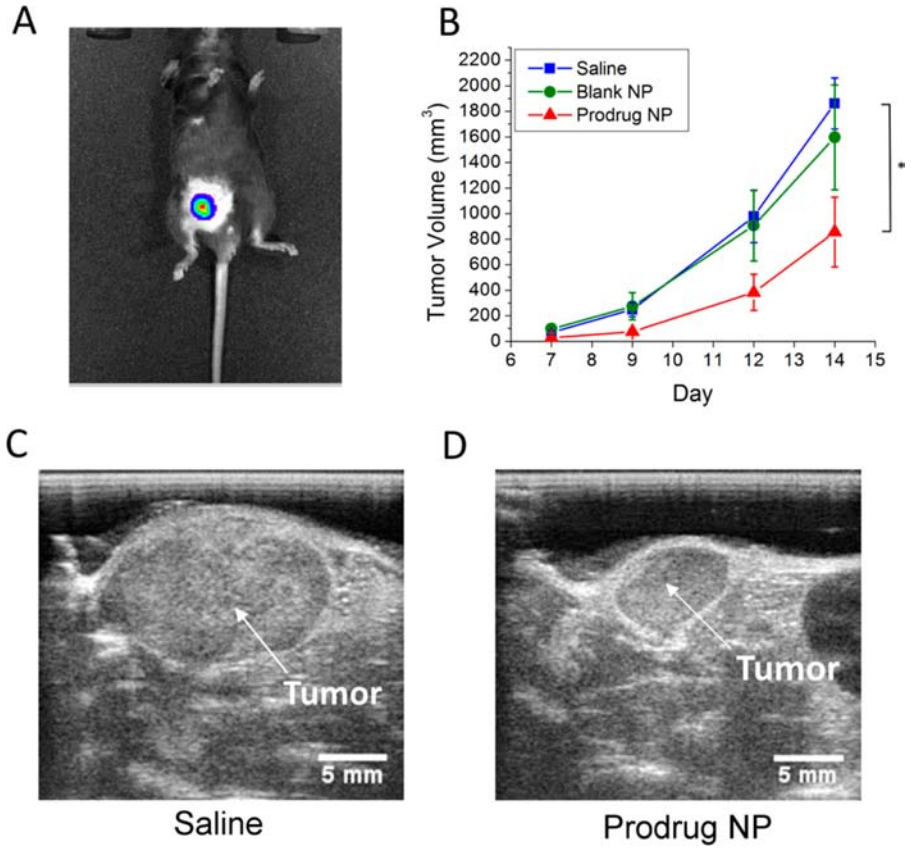

Figure 5. Efficacy of prodrug-loaded nanoparticles in a mouse model of melanoma. (A) Bioluminescence image demonstrating the location of a subcutaneously implanted tumor in the right inguinal region on day 7 postimplantation. (B) Time course of tumor growth in treated mice as determined by serial ultrasound measurements. Error bars represent standard error of $n = 5$ replicates. Label indicates level of statistical significance compared to saline control: *, $p < 0.05$. (C and D) Sample ultrasound images demonstrating the location and size of tumors in mice treated with saline and prodrug-loaded nanoparticles on day 14 postimplantation.

prodrug-loaded nanoparticles as cytolytic agents for cells producing MMP-9.

Activity in a Mouse Model of Melanoma. To demonstrate the utility of the melittin prodrug platform in vivo, we used a syngeneic mouse cancer model in which B16F10 melanoma cells expressing luciferase were implanted subcutaneously into the inguinal region of C57BL/6 mice (Figure 5A). Importantly, this model allows tumor growth in mice possessing competent immune systems and results in tumors expressing substantial levels of both latent and active MMP-9 (Figure S2). Mice were treated with four intravenous injections of saline, blank nanoparticles, or prodrug-loaded nanoparticles (1 mg/kg), and tumor growth was assessed by serial ultrasound measurements. Treatment with prodrug-loaded nanoparticles resulted in a significant decrease in tumor growth rate compared to the effect of saline and blank nanoparticle treatment (~54% reduction in tumor size at day 14; $p = 0.01$; Figures 5B–D). This result compares favorably with the ~52% decrease in tumor size observed with an equivalent dose of melittin-loaded nanoparticles in a previous study.[3] Importantly, increasing the melittin-loaded nanoparticle dose to 8 mg/kg further enhanced tumor growth inhibition in this prior report (~88% reduction in tumor size at day 14), suggesting that an increased dose of prodrug-loaded nanoparticles could also be more effective at suppressing tumor growth. As with melittin-loaded nanoparticles, mice treated with prodrug-loaded nanoparticles were asymptomatic following all treatments and analysis of blood cells, serum electrolytes, and liver and kidney function revealed only a slight, nonsignificant decrease in white blood cell count following treatment with prodrug-loaded nanoparticles ($p = 0.088$; Table S1). Similarly, blank nanoparticles and prodrug-loaded nanoparticles induced minimal levels of complement activation following intravenous administration (Figure S3), further attesting to their potential safety as systemic therapies. We expect that the impact of prodrug-loaded nanoparticles on reducing tumor growth could be further optimized by alterations in dosing, prodrug sequence, and tumor targeting through the use of well-established nanoparticle modifications.[35]

■ CONCLUSIONS

We have developed an MMP-9-activated derivative of melittin that is based on the structure of honeybee promelittin. To our knowledge, this is the first report of such a prodrug melittin system being delivered safely on a stable perfluorocarbon nanostructure that serves to protect the peptide in the circulation and deliver it to tissue sites for selective local activation by tumor cells. This prodrug demonstrates efficacy in both cell culture and animal models of MMP-9 production. The platform we describe may be readily applied to generate melittin derivatives activated by a variety of other proteases and may hold promise for the development of personalized cancer therapies that can be targeted to a patient's individual protease expression profile.

DOI: 10.1021/acs.bioconjchem.5b00246
Bioconjugate Chem. 2015, 26, 1640–1650

EXPERIMENTAL PROCEDURES

Peptide Synthesis. All peptides were generated commercially using solid-phase peptide synthesis. Melittin was produced by GenScript (Piscataway, NJ), whereas Pro-P1 and Pro-P2 were produced by American Peptide Company (Sunnyvale, CA).

Cell Culture and Viability. 2F2B endothelial cells (CRL-2168), RAW 264.7 macrophages (TIB-71), and B16F10 melanoma cells (CRL-6475) were obtained from ATCC (Manassas, VA) and propagated according to the suggested protocol using Dulbecco's modified Eagle's medium (DMEM) supplemented with 10% fetal bovine serum (Life Technologies, Carlsbad, CA). For cytotoxicity studies, 15 000 cells (2F2B and B16F10) or 30 000 cells (RAW 264.7) were added to each well of a 96-well plate and allowed to attach overnight. The agent of interest was then added and incubated with the cells for 3 h (free peptide) or 24 h (nanoparticle-bound peptide) at 37 °C. Following incubation, cells were washed once with PBS (Life Technologies, Carlsbad, CA) and viability was assessed using the XTT assay (Biotium, Hayward, CA) according to the manufacturer's instructions. Briefly, activated XTT solution was incubated with the cells for 5 h and absorbance at 450 nm (reference wavelength: 630 nm) was measured using a plate reader. To determine percent viability, absorbance readings were normalized to those of untreated cells.

For studies involving stimulation with TNF-α and MMP-3, 15 000 cells were added to each well of a 96-well plate and allowed to attach overnight. The media was then replaced with serum-free DMEM containing 100 ng/mL TNF-α (R&D Systems, Minneapolis, MN), and cells were incubated at 37 °C for 24 h. Activated MMP-3 (R&D Systems, Minneapolis, MN) was then added to a final concentration of 10 nM along with the agent of interest and incubated with the cells for 3 h (free peptide) or 24 h (nanoparticle-bound peptide) at 37 °C. The media was then removed, cells washed once with PBS, and viability assessed using the XTT assay.

Hemolysis Assay. Citrated whole blood was collected from New Zealand white rabbits and separated by centrifugation at 2000 rpm for 10 min. Red blood cells were washed five times with PBS and stored at 4 °C until use. For each assay, the agent of interest was added to 1×10^7 red blood cells in PBS and incubated at 37 °C for 1 h. Afterward, intact red blood cells were pelleted by centrifugation at 2000 rpm for 5 min, and absorbance of the supernatant was measured at 450 nm (reference wavelength: 630 nm). To determine percent lysis, absorbance readings were normalized to lysis with 0.1% Triton X-100.

MMP Cleavage. Recombinant mouse MMP-9 and MMP-3 were purchased from R&D Systems (Minneapolis, MN) and activated on the day of use by incubating with 1 mM 4-aminophenylmercuric acetate (APMA, Sigma-Aldrich, St. Louis, MO) at 37 °C for 2 h in TCNBZ buffer (150 mM NaCl, 50 mM Tris, 10 mM $CaCl_2$, 10 μM $ZnCl_2$, and 0.05% (w/v) Brij-35, pH 7.75). Free APMA was removed by dialysis against TCNBZ buffer for 2 h using a Slide-A-Lyzer MINI Dialysis Device, 2K MWCO (Life Technologies, Carlsbad, CA) with a dialysate change at 1 h. Peptide cleavage by MMP-9 was performed by incubating the agent of interest with 20 nM activated MMP-9 in TCNBZ buffer for 3 h at 37 °C. Activated MMP-3 was added to the media of TNF-α stimulated cells at a final concentration of 10 nM.

HPLC Analysis. Reversed-phase high-performance liquid chromatography (HPLC) of peptide mixtures was performed using a Waters HPLC system (Waters Corporation, Milford, MA) and a Vydac 218TP54 (C18) column (Discovery Sciences, Albany, OR). The mobile phase consisted of a mixture of 0.1% trifluoroacetic acid (TFA) in water (solvent A) and 0.1% TFA in acetonitrile (solvent B). Composition of the mobile phase was varied from 60% buffer A/40% buffer B to 40% buffer A/60% buffer B over the course of 20 min. A flow rate of 1.2 mL/min and injection volume of 20 μL were used. For analysis of nanoparticle-bound peptides, nanoparticles were first treated with an equal volume of isopropanol and centrifuged at 5000 rpm for 1 min to remove the perfluorocarbon. An injection volume of 40 μL was used to compensate for peptide dilution. Eluting peptides were detected by absorbance at 215 nm. To determine the concentration of eluting peptide, the area underneath the HPLC peak was compared to a standard curve generated using known concentrations of the peptide.

Mass Spectrometry. Fractions containing peptides of interest were collected following separation by HPLC. A 1 mL aliquot of each fraction was dried down and resuspended in 50 μL of 50% methanol/0.1% formic acid solution. Samples were infused using a TriVersa NanoMate (Advion, Ithaca, NY), and data were acquired from an LTQ-Velos Pro Orbitrap LC-MS/MS mass spectrometer (Thermo Scientific, Waltham, MA) over a 3 min run including MS and MS2 (CID) scans.

All MS/MS data were analyzed using Mascot software (Matrix Science, London, UK; version 2.4.1). Mascot was set up to search a custom database including the expected peptide sequence and nonspecific degradation products. Mascot was searched with a fragment ion mass tolerance of 0.80 Da and a parent ion tolerance of 15 ppm. Scaffold software (Proteome Software Inc., Portland, OR; version 4.3.2) was used to validate MS/MS-based peptide identifications. Peptide identifications were accepted if they could be established at greater than 95.0% probability by the Peptide Prophet algorithm[36] with Scaffold delta-mass correction.

Gelatin Zymography. Gelatin zymography was performed using precast Novex Zymogram Gels (Life Technologies, Carlsbad, CA) according to the manufacturer's instructions. Briefly, 20 μL of serum-free conditioned media or 20 μg of tumor lysate protein were loaded into each well of a Novex Zymogram Gel containing 10% gelatin. A Precision Plus Protein Kaleidoscope ladder (Bio-Rad, Hercules, CA) was used as a molecular weight standard. The gel was run at 125 V for 115 min, incubated in Zymogram Renaturing Buffer (Life Technologies, Carlsbad, CA) for 30 min and then incubated overnight at 37 °C in Zymogram Developing Buffer (Life Technologies, Carlsbad, CA). The gel was then stained using Coomassie SimplyBlue SafeStain (Life Technologies, Carlsbad, CA) according to the manufacturer's instructions and imaged using a Chemidoc gel-imaging system (Bio-Rad, Hercules, CA).

Nanoparticle Synthesis and Loading. Perfluorocarbon nanoparticles were synthesized as previously described.[37] Briefly, a lipid surfactant mixture of egg phosphatidylcholine (90 mol %) and dipalmitoylphosphatidylglycerol (10 mol %) (Avanti Polar Lipids, Piscataway, NJ) was dissolved in chloroform, evaporated under reduced pressure, and dried in a 50 °C vacuum oven. This lipid composition was chosen to optimize loading and cleavage of the prodrug. For comparison with previous studies,[3,9] nanoparticles loaded with melittin contained a lipid surfactant layer composed of egg

DOI: 10.1021/acs.bioconjchem.5b00246
Bioconjugate Chem. 2015, 26, 1640−1650

phosphatidylcholine (98 mol %) and dipalmitoylphosphatidylethanolamine (2 mol %). The resulting lipid film (2% w/v) was resuspended in distilled deionized water and combined with perfluorooctyl bromide (Gateway Specialty Chemicals, St. Peters, MO) (20% w/v). This mixture was sonicated three times for 15 seconds each using a Sonifier 250 ultrasonic homogenizer (Branson Ultrasonics Corporation, Danbury, CT) and then passed five times through an LV1 microfluidizer (Microfluidics Corporation, Westwood, MA) at 20 000 psi to obtain an emulsion of perfluorocarbon nanoparticles. Nanoparticles were stored in PBS at 4 °C until use.

Melittin and prodrug loading was accomplished by incubating nanoparticles with 1 mM of the appropriate peptide in PBS for 1 h at 4 °C. Nanoparticles were then isolated by centrifugation at 3000g for 15 min. The supernatant was removed, and nanoparticles were washed three times with PBS to remove free peptide.

Nanoparticle Characterization. Nanoparticle size and zeta potential were determined using a ZetaPlus Zeta Potential analyzer (Brookhaven Instruments Corporation, Holtsville, NY). The average nanoparticle diameter was used to calculate average nanoparticle volume assuming a spherical geometry. Given that the perfluorocarbon core constitutes the vast majority of nanoparticle volume, the volume of liquid perfluorocarbon initially used in the synthesis was divided by the average nanoparticle volume to estimate the number of nanoparticles present following synthesis. This number was divided by the total volume of the suspension to determine nanoparticle concentration. Following melittin or prodrug loading, the peptide concentration as determined by HPLC was divided by nanoparticle concentration to estimate the number of peptides bound per nanoparticle.

Loading efficiency is a metric used to characterize the percentage of melittin or prodrug initially added to nanoparticles that remains following washing and removal of unbound peptide. To calculate this value, the final nanoparticle-bound peptide concentration was divided by the initial peptide concentration used to load the nanoparticles.

Peptide Release Kinetics. Nanoparticles loaded with melittin or prodrug at a concentration of 50 μM were dialyzed against 1 L of PBS for 48 h using a Micro Float-A-Lyzer device with MWCO 100 kDa (Spectrum Laboratories, Rancho Dominguez, CA).The dialysate was replaced every 24 h. At selected time points (3, 6, 12, 24, and 48 h), nanoparticle aliquots were withdrawn, and the remaining melittin or prodrug content was determined by HPLC. This value was normalized by the melittin or prodrug content of undialyzed nanoparticles to calculate the percent retention at each time point.

Peptide Cleavage Kinetics. Free prodrug or prodrug-loaded nanoparticles at a concentration of 50 μM were added to active recombinant MMP-9 (2, 5, 10, 15, or 20 nM) in TCNBZ buffer and incubated at 37 °C. At the appropriate time point, 1 μM prinomastat was added to stop the reaction, and HPLC analysis of the peptide mixture was performed. To determine percent cleavage, the concentration of uncleaved prodrug in each sample was compared to a control sample that did not contain MMP-9. An exponential curve of the form

$$\%\ \text{Cleaved} = 100(1 - e^{-kt})$$

where k is a rate constant (s^{-1}) was fitted to the time course for each MMP-9 concentration. The initial cleavage rate was calculated as

$$V_0 = k[S_0]$$

where $[S_0]$ is the initial prodrug concentration (50 μM). The initial cleavage rate was then plotted as a function of MMP-9 concentration and used to calculate an effective k_{cat}/K_m value using the linear initial velocity version of the Michaelis–Menten equation:[38]

$$V_0 = \frac{k_{cat}}{K_m}[E][S_0]$$

Melanoma Mouse Model. All animal protocols were approved by the Washington University Animal Studies Committee. Mice were housed in standard 9 × 15 × 6 $in.^3$ mouse cages (3–5 per cage) and were fed with rodent chow and water. C57BL/6 mice (4–6 weeks old; Harlan Laboratories, Indianapolis, IN) were randomized into treatment groups receiving prodrug-loaded nanoparticles (1 mg/kg per dose), blank nanoparticles, or saline. They were then implanted subcutaneously in the right inguinal region with 1×10^6 B16F10-lucG5 cells and treated by tail vein injection of the appropriate agent on days 5, 7, 9, and 12 postimplantation. Bioluminescence and ultrasound imaging were performed on days 7, 9, 12, and 14, and mice were sacrificed on day 14. Following sacrifice, blood was collected by left ventricular puncture for biochemical analysis, and the tumor was removed and snap-frozen in liquid nitrogen for analysis of MMP activity.

To prepare tumor lysates for gelatin zymography, snap-frozen tumors were homogenized in lysis buffer using a Bullet Blender tissue homogenizer (Next Advance, Averill Park, NY). Lysis buffer was composed of 100 mM NaCl, 25 mM Tris-HCl, pH 7.5, and 1% v/v Nonidet P-40 with the addition of 1 cOmplete, Mini, EDTA-free protease-inhibitor cocktail tablet (Roche, Pleasanton, CA) per 10 mL of lysis buffer immediately before use. The tumor lysate was centrifuged at 16 000g for 10 min at 4 °C, and the supernatant was collected for analysis. Protein concentration in the supernatant was determined by BCA assay (Life Technologies, Carlsbad, CA) according to the manufacturer's instructions.

Bioluminescence Imaging. Prior to imaging, the area surrounding the tumor was shaved and depilated using surgical depilatory cream. Mice were injected intraperitoneally with 150 mg/kg D-luciferin (Sigma-Aldrich, St. Louis, MO) in sterile saline. Thirty minutes following injection, mice were anesthetized with isoflurane and imaged using an IVIS Spectrum in vivo imaging system (PerkinElmer, Waltham, MA) in luminescence mode.

Ultrasound Imaging. Tumor growth was confirmed by in vivo transcutaneous imaging with high-frequency ultrasound systems. Two systems were used, each having a specific tumor size range over which imaging was optimal. For tumors less than 1 cm in diameter, a high-frequency, mechanically scanned, single-element imaging system was employed (Vevo 660, VisualSonics, Toronto, Ontario, Canada), whereas a linear array (Spark High Frequency Imaging System, Ardent Sound, Mesa, AZ) was used to image larger tumors. Probes used were the RMV-703 (35 MHz) for the Vevo system and a high-frequency (nominal 15 MHz) linear array for the Spark system. Both systems were modified to output analog radiofrequency (rf) data (beamformed A-lines for the Spark system) and associated trigger signals in order to permit digitization of the raw backscattered rf waveforms from the mouse tumors.

Prior to scanning, each animal was anesthetized with isoflurane and the area around the tumor shaved and depilated.

DOI: 10.1021/acs.bioconjchem.5b00246
Bioconjugate Chem. 2015, 26, 1640–1650

The transducers were affixed to a motorized gantry under computer control in order to enable automated scanning of the probe across the length of the tumor. Each anesthetized animal was placed on its back on a heated platform beneath the probe, and a small amount of ultrasound coupling gel was applied to the area proximal to the tumor. The probe was positioned so that the central area of the tumor was situated in the focal region of the transducer. The rf data corresponding to cross-sectional views of the tumor were acquired at multiple sites along the length of the tumor so that the entire tumor volume was interrogated. The probe was translated laterally (perpendicular to the transducer's imaging plane) in 100 μm steps between each scan plane acquisition. Subsequent to acquisition, the envelope of each rf waveform was used to create gray-scale images. All computation, image reconstruction, and image analysis was performed using custom Java plugins written for the open-source image analysis package ImageJ (National Institutes of Health, Bethesda, MD). User-specified regions of interest (ROIs) were drawn on each image frame, and the area of the ROI measured. The areas of the ROIs were multiplied by the distance between scan planes to yield subvolumes, which were summed to compute the entire tumor volume.

Complement Activation. The extent of complement activation following nanoparticle injection was determined by C3a ELISA as reported previously.[39,40] Briefly, wild-type C57BL/6J mice were injected with 30 μL of nanoparticles or PBS (negative control). After 30 min, their plasma was collected in EDTA-containing tubes to inhibit further ex vivo complement activation. For the ELISA, plates were coated overnight at 4 °C with anti-mouse C3a (4 μg/mL) monoclonal antibody (BD Pharmingen, San Jose, CA). After being blocked with 1% BSA, the plates were washed and incubated with samples (100 μL of fresh plasma diluted 1:100 in 1% BSA in PBS) for 2 h at room temperature, followed by biotinylated anti-mouse C3a (250 ng/mL) monoclonal antibody (BD Pharmingen). After washes and incubation with streptavidin−peroxidase (400 ng/mL; Sigma-Aldrich, St. Louis, MO), 100 μL of peroxide−chromogen solution (R&D Systems, Minneapolis, MN) was added to each well, and color development was read at 450 nm with a SpectraMax Plus reader (Molecular Devices, Sunnyvale, CA). Mouse recombinant C3a (BD Pharmingen) was used to establish the standard curve. N-[1-(2,3-Dioleoyloxy)propyl]-N,N,N- trimethylammonium methylsulfate (DOTAP, 50 mol %) nanoparticles served as positive controls for robust complement activation.

Statistical Analysis. Data are represented as mean ± standard deviation of at least three independent samples unless otherwise indicated. For in vitro assays, an unpaired two-tailed Student's t test was performed assuming a normal sample distribution. For in vivo studies, an analysis of covariance (ANCOVA) was used to assess the effect of treatment on tumor growth rate. Values of $p < 0.05$ were considered statistically significant for all comparisons. For cytotoxicity and hemolysis assays, a four-parameter logistic curve was fit to the data using a nonlinear least-squares technique and used to determine peptide concentrations resulting in 50% cytotoxicity or hemolysis. The standard errors of these values were then determined using the delta method.[41]

■ ASSOCIATED CONTENT

Supporting Information

Prinomastat inhibition of prodrug cleavage, MMP-9 expression by melanoma tumors, biochemical studies, and complement activation in treated mice. The Supporting Information is available free of charge on the ACS Publications website at DOI: 10.1021/acs.bioconjchem.5b00246.

■ AUTHOR INFORMATION

Corresponding Author

*Washington University School of Medicine, Box 8215, 660 South Euclid Avenue, St. Louis, MO 63110. Phone: (314) 454-8811. E-mail: wicklines@aol.com.

Notes

The authors declare no competing financial interest.

■ ACKNOWLEDGMENTS

This work was supported by grants from the National Institutes of Health (NIH R01 HL073646 and U54 HL112303), the Barnes-Jewish Hospital Foundation, and the James R. Hornsby Family Dream Garden Investment Partnership to S.A.W. We thank Stacy Allen for general assistance with animal studies, Luke Springer for performing the complement activation assays, and Dr. Sophie Alvarez and the Proteomics Facility at The Donald Danforth Plant Science Center, St. Louis, MO, for assistance with mass spectrometry. The mass spectrometry result is based upon work supported by the National Science Foundation under grant no. DBI-0922879 for acquisition of the LTQ-Velos Pro Orbitrap LC-MS/MS.

■ REFERENCES

(1) Shai, Y. (1999) Mechanism of the Binding, Insertion and Destabilization of Phospholipid Bilayer Membranes by A-Helical Antimicrobial and Cell Non-Selective Membrane-Lytic Peptides. *Biochim. Biophys. Acta, Biomembr. 1462*, 55−70.

(2) Mader, J. S., and Hoskin, D. W. (2006) Cationic Antimicrobial Peptides as Novel Cytotoxic Agents for Cancer Treatment. *Expert Opin. Invest. Drugs 15*, 933−946.

(3) Soman, N. R., Baldwin, S. L., Hu, G., Marsh, J. N., Lanza, G. M., Heuser, J. E., Arbeit, J. M., Wickline, S. A., and Schlesinger, P. H. (2009) Molecularly Targeted Nanocarriers Deliver the Cytolytic Peptide Melittin Specifically to Tumor Cells in Mice, Reducing Tumor Growth. *J. Clin. Invest. 119*, 2830−2842.

(4) Findlay, B., Zhanel, G. G., and Schweizer, F. (2010) Cationic Amphiphiles, a New Generation of Antimicrobials Inspired by the Natural Antimicrobial Peptide Scaffold. *Antimicrob. Agents Chemother. 54*, 4049−4058.

(5) Fjell, C. D., Hiss, J. A., Hancock, R. E. W., and Schneider, G. (2012) Designing Antimicrobial Peptides: Form Follows Function. *Nat. Rev. Drug Discovery 11*, 37−51.

(6) Hood, J. L., Jallouk, A. P., Campbell, N., Ratner, L., and Wickline, S. A. (2013) Cytolytic Nanoparticles Attenuate HIV-1 Infectivity. *Antiviral Ther. 18*, 95−103.

(7) Galdiero, S., Falanga, A., Tarallo, R., Russo, L., Galdiero, E., Cantisani, M., Morelli, G., and Galdiero, M. (2013) Peptide Inhibitors against Herpes Simplex Virus Infections. *J. Pept. Sci. 19*, 148−158.

(8) Schweizer, F. (2009) Cationic Amphiphilic Peptides with Cancer-Selective Toxicity. *Eur. J. Pharmacol. 625*, 190−194.

(9) Soman, N. R., Lanza, G. M., Heuser, J. M., Schlesinger, P. H., and Wickline, S. A. (2008) Synthesis and Characterization of Stable Fluorocarbon Nanostructures as Drug Delivery Vehicles for Cytolytic Peptides. *Nano Lett. 8*, 1131−1136.

(10) Huang, C., Jin, H., Qian, Y., Qi, S., Luo, H., Luo, Q., and Zhang, Z. (2013) Hybrid Melittin Cytolytic Peptide-Driven Ultrasmall Lipid Nanoparticles Block Melanoma Growth in Vivo. *ACS Nano 7*, 5791−5800.

(11) Falco, A., Barrajón-Catalán, E., Menéndez-Gutiérrez, M. P., Coll, J., Micol, V., and Estepa, A. (2013) Melittin-Loaded Immunoliposomes against Viral Surface Proteins, a New Approach to Antiviral Therapy. *Antiviral Res. 97*, 218−221.

DOI: 10.1021/acs.bioconjchem.5b00246
Bioconjugate Chem. 2015, 26, 1640−1650

(12) Jallouk, A. P., Moley, K. H., Omurtag, K., Hu, G., Lanza, G. M., Wickline, S. A., and Hood, J. L. (2014) Nanoparticle Incorporation of Melittin Reduces Sperm and Vaginal Epithelium Cytotoxicity. *PLoS One 9*, e95411.
(13) Holle, L., Song, W., Holle, E., Wei, Y., Wagner, T. E., and Yu, X. (2003) A Matrix Metalloproteinase 2 Cleavable Melittin/avidin Conjugate Specifically Targets Tumor Cells in Vitro and in Vivo. *Int. J. Oncol. 22*, 93−98.
(14) Holle, L., Song, W., Holle, E., Wei, Y., Li, J., Wagner, T. E., and Yu, X. (2009) In Vitro- and in Vivo-Targeted Tumor Lysis by an MMP2 Cleavable Melittin-LAP Fusion Protein. *Int. J. Oncol. 35*, 829−835.
(15) LeBeau, A. M., Brennen, W. N., Aggarwal, S., and Denmeade, S. R. (2009) Targeting the Cancer Stroma with a Fibroblast Activation Protein-Activated Promelittin Protoxin. *Mol. Cancer Ther. 8*, 1378−1386.
(16) Desgranges, S., Prieult, F. L., Daly, A., Lydon, J., Brennan, M., Rai, D. K., Subasinghage, A. P., Hewage, C. M., Cryan, S.-A., Greene, C., et al. (2011) In Vitro Activities of Synthetic Host Defense Propeptides Processed by Neutrophil Elastase against Cystic Fibrosis Pathogens. *Antimicrob. Agents Chemother. 55*, 2487−2489.
(17) Kreil, G., Haiml, L., and Suchanek, G. (1980) Stepwise Cleavage of the Pro Part of Promelittin by Dipeptidylpeptidase IV. *Eur. J. Biochem. 111*, 49−58.
(18) Deryugina, E. I., and Quigley, J. P. (2006) Matrix Metalloproteinases and Tumor Metastasis. *Cancer Metastasis Rev. 25*, 9−34.
(19) Shuman Moss, L. A., Jensen-Taubman, S., and Stetler-Stevenson, W. G. (2012) Matrix Metalloproteinases: Changing Roles in Tumor Progression and Metastasis. *Am. J. Pathol. 181*, 1895−1899.
(20) Schilsky, R. L. (2010) Personalized Medicine in Oncology: The Future Is Now. *Nat. Rev. Drug Discovery 9*, 363−366.
(21) Meric-Bernstam, F., and Mills, G. B. (2012) Overcoming Implementation Challenges of Personalized Cancer Therapy. *Nat. Rev. Clin. Oncol. 9*, 542−548.
(22) Forde, É., Humphreys, H., Greene, C. M., Fitzgerald-Hughes, D., and Devocelle, M. (2014) Potential of Host Defense Peptide Prodrugs as Neutrophil Elastase-Dependent Anti-Infective Agents for Cystic Fibrosis. *Antimicrob. Agents Chemother. 58*, 978−985.
(23) Netzel-Arnett, S., Sang, Q. X., Moore, W. G. I., Navre, M., Birkedal-Hansen, H., and Van Wart, H. E. (1993) Comparative Sequence Specificities of Human 72- and 92-kDa Gelatinases (type IV Collagenases) and PUMP (matrilysin). *Biochemistry (Moscow, Russ. Fed.) 32*, 6427−6432.
(24) Nagase, H., and Fields, G. B. (1996) Human Matrix Metalloproteinase Specificity Studies Using Collagen Sequence-Based Synthetic Peptides. *Pept. Sci. 40*, 399−416.
(25) Nagase, H. (2001) Substrate Specificity of MMPs. In *Matrix Metalloproteinase Inhibitors in Cancer Therapy* (Clendeninn, N. J., and Appelt, K., Eds.) pp 39−66, Cancer Drug Discovery and Development Series, Humana Press, Totowa, NJ.
(26) Hanash, S., and Schliekelman, M. (2014) Proteomic Profiling of the Tumor Microenvironment: Recent Insights and the Search for Biomarkers. *Genome Med. 6*, 1−12.
(27) Sanman, L. E., and Bogyo, M. (2014) Activity-Based Profiling of Proteases. *Annu. Rev. Biochem. 83*, 249−273.
(28) Jallouk, A. P., Palekar, R. U., Pan, H., Schlesinger, P. H., and Wickline, S. A. (2015) Modifications of Natural Peptides for Nanoparticle and Drug Design. In *Protein and Peptide Nanoparticles for Drug Delivery* (Donev, R., Ed.) pp 57−91, Chapter 2, Advances in Protein Chemistry and Structural Biology Series, Vol. *98*, Academic Press, Boston, MA.
(29) Kuchinka, E., and Seelig, J. (1989) Interaction of Melittin with Phosphatidylcholine Membranes. Binding Isotherm and Lipid Head-Group Conformation. *Biochemistry (Moscow, Russ. Fed.) 28*, 4216−4221.
(30) Kim, A., Son, M., Kim, K. I., Yang, Y., Song, E. Y., Lee, H. G., and Lim, J.-S. (2009) Elevation of Intracellular Cyclic AMP Inhibits NF-κB-Mediated Thymosin β4 Expression in Melanoma Cells. *Exp. Cell Res. 315*, 3325−3335.
(31) Ogata, Y., Enghild, J. J., and Nagase, H. (1992) Matrix Metalloproteinase 3 (stromelysin) Activates the Precursor for the Human Matrix Metalloproteinase 9. *J. Biol. Chem. 267*, 3581−3584.
(32) Ramos-DeSimone, N., Hahn-Dantona, E., Sipley, J., Nagase, H., French, D. L., and Quigley, J. P. (1999) Activation of Matrix Metalloproteinase-9 (MMP-9) via a Converging Plasmin/Stromelysin-1 Cascade Enhances Tumor Cell Invasion. *J. Biol. Chem. 274*, 13066−13076.
(33) Boles, K. S., Schmieder, A. H., Koch, A. W., Carano, R. A. D., Wu, Y., Caruthers, S. D., Tong, R. K., Stawicki, S., Hu, G., Scott, M. J., et al. (2010) MR Angiogenesis Imaging with Robo4- vs. αVβ3-Targeted Nanoparticles in a B16/F10 Mouse Melanoma Model. *FASEB J. 24*, 4262−4270.
(34) Wolfe, C., Cladera, J., and O'Shea, P. (1998) Amino Acid Sequences Which Promote and Prevent the Binding and Membrane Insertion of Surface-Active Peptides: Comparison of Melittin and Promelittin. *Mol. Membr. Biol. 15*, 221−227.
(35) Wickline, S. A., and Lanza, G. M. (2003) Nanotechnology for Molecular Imaging and Targeted Therapy. *Circulation 107*, 1092−1095.
(36) Keller, A., Nesvizhskii, A. I., Kolker, E., and Aebersold, R. (2002) Empirical Statistical Model To Estimate the Accuracy of Peptide Identifications Made by MS/MS and Database Search. *Anal. Chem. 74*, 5383−5392.
(37) Winter, P. M., Caruthers, S. D., Kassner, A., Harris, T. D., Chinen, L. K., Allen, J. S., Lacy, E. K., Zhang, H., Robertson, J. D., Wickline, S. A., et al. (2003) Molecular Imaging of Angiogenesis in Nascent Vx-2 Rabbit Tumors Using a Novel αvβ3-Targeted Nanoparticle and 1.5 T Magnetic Resonance Imaging. *Cancer Res. 63*, 5838−5843.
(38) Neumann, U., Kubota, H., Frei, K., Ganu, V., and Leppert, D. (2004) Characterization of Mca-Lys-Pro-Leu-Gly-Leu-Dpa-Ala-Arg-NH_2, a Fluorogenic Substrate with Increased Specificity Constants for Collagenases and Tumor Necrosis Factor Converting Enzyme. *Anal. Biochem. 328*, 166−173.
(39) Zhou, H., Yan, H., Senpan, A., Wickline, S. A., Pan, D., Lanza, G. M., and Pham, C. T. N. (2012) Suppression of Inflammation in a Mouse Model of Rheumatoid Arthritis Using Targeted Lipase-Labile Fumagillin Prodrug Nanoparticles. *Biomaterials 33*, 8632−8640.
(40) Wang, K., Pan, D., Schmieder, A. H., Senpan, A., Hourcade, D. E., Pham, C. T. N., Mitchell, L. M., Caruthers, S. D., Cui, G., Wickline, S. A., et al. (2015) Synergy between Surface and Core Entrapped Metals in a Mixed Manganese−gadolinium Nanocolloid Affords Safer MR Imaging of Sparse Biomarkers. *Nanomedicine (N.Y., NY, U.S.) 11*, 601−609.
(41) Cox, C. (2005) Delta Method. In *Encyclopedia of Biostatistics* (Armitage, P., and Colton, T., Eds.) B2A15029, John Wiley & Sons, Ltd, Chichester, West Sussex, United Kingdom.

DOI: 10.1021/acs.bioconjchem.5b00246
Bioconjugate Chem. 2015, 26, 1640−1650